ISSN (Print) 1226-1750
ISSN (Online) 2233-6656
Journal of Magnetics 19(1), 84-89 (2014) http://dx.doi.org/10.4283/JMAG.2014.19.1.084

Analytical Prediction and Experimental Verification of Electromagnetic Performance of a Surface-Mounted Permanent Magnet Motor having a Fractional Slot/Pole Number Combination

Sang-A Hong, Jang-Young Choi*, and Seok-Myeong Jang

Department of Electrical Engineering, Chungnam National University, Daejeon 305-764, Korea

(Received 27 September 2013, Received in final form 21 November 2013, Accepted 22 November 2013)

This paper presents an analytical prediction and experimental verification of the electromagnetic performance of a parallel magnetized surface-mounted permanent magnet (SPM) motor having a fractional number of slots per pole combination. On the basis of a two-dimensional (2-D) polar coordinate system and a magnetic vector potential, analytical solutions for flux density produced by the permanent magnets (PMs) and stator windings are derived. Then, analytical solutions for back-electromotive force (emf) and electromagnetic torque are derived from these field solutions. The analytical results are thoroughly validated with 2-D nonlinear finite element (FE) analysis results. Finally, the experimental back-emf and electromagnetic torque measurements are presented to test the validity of the analysis.

Keywords : surface-mounted permanent magnet motor, fractional number of slots per pole combination, analytical solutions

1. Introduction

A permanent magnet, which has good efficiency over a wide range of operations, is preferable for various electrical machine applications [1]. Surface-mounted permanent magnet (SPM) motors, in particular, have a simple structure, low cost, and high power density [2]. Moreover, their power density can be improved by increasing the number of poles. However, this leads to an increase in the number of slots, which increases the machine size and cogging torque. A fractional-slot SPM motor with a multipole permanent magnet (PM) rotor has a more sinusoidal back-electromotive force (emf), high torque density, and small cogging torque [3]. However, the asymmetric layout of its stator windings produces many space harmonics magnetomotive force (mmf) [4], resulting in an increase in vibration and noise of the SPM motor. Therefore, there has been increased attention on the electromagnetic analysis of this motor.

For the electromagnetic analysis, involving back-emf and electromagnetic torque, of the fractional slot/pole SPM motor, accurate calculations of the magnetic field distribution generated by the PMs and stator winding currents are essential. A magnetic field analysis using the space harmonic method and the finite element (FE) method is preferred. Although the FE analysis method provides accurate results, it is often time consuming and has poor flexibility.

In this paper an analytical prediction and experimental verification of the electromagnetic performance of an SPM motor having fractional slot/pole number combinations (6-pole rotor and 27-slot stator) are discussed. The analytical solution of the open-circuit and armature-reaction fields distributed at different radii is based on a two-dimensional (2-D) polar coordinate system and a magnetic vector potential. It involves a governing equation for air-gap and PM regions with parallel magnetization. Thus, the analytical solutions for the back-emf and electromagnetic torque are also established from the solutions for flux density produced by the PMs and stator winding currents. In addition, the analytical results are extensively validated with the nonlinear FE results. Finally, test results such as back-emf and torque measurements are also provided to confirm the analytical results.

*Corresponding author: Tel: +82-42-821-7610
Fax: +82-42-822-4933, e-mail: choi_jy@cnu.ac.kr

2. Formula Problem

2.1. Analytical Model

Figures 1(a) and 1(b) show a schematic of the SPM motor having a 6-pole PM rotor and a 27-slot stator and a photograph of the actual fixture model, respectively. As shown in Fig. 1(a), the stator coils are wound around each tooth with a double-layer winding, and the stator windings per phase are asymmetric because of the fractional slot/pole number combination. To predict analytical solutions, we are based on several assumptions [5]. The permeability of the stator and rotor core is infinite, the relative permeability of the PM is unity, and the stator windings are distribute as a current sheet on the inner radius of the stator. The coordinate frame has (r, θ, z) and (r, α, z) as coordinates of the rotor and stator, respectively. Further, θ and α are related as $\theta = \alpha + \omega_r t$, where ω_r is the angular speed of the rotor in radians per second.

2.2. Magnetic Fields Produced by PMs

In the PM region, the magnetic flux density is given as $\mathbf{B} = \mu_0(\mathbf{H} + \mathbf{M})$ and $\nabla \times \mathbf{H} = 0$ because there is no current. Then, $\nabla \times \mathbf{B} = \mu_0(\nabla \times \mathbf{M})$. The magnetic vector potential is defined as $\nabla \times \mathbf{A} = \mathbf{B}$. Thus, using the Coulomb gauge $\nabla \cdot \mathbf{A} = 0$, the Laplace's and Poisson's equations for each region are given by

$$\begin{aligned} \nabla^2 \mathbf{A}^{pm\mathrm{I}} &= 0 \\ \nabla^2 \mathbf{A}^{pm\mathrm{II}} &= -\mu_0 (\nabla \times \mathbf{M}) \end{aligned} \tag{1}$$

where μ_0 is the permeability of air. Figure 3 shows the parallel magnetization model of Fourier series expansion of the PMs [6]. Here, θ_m is angle for one pole of the PMs,

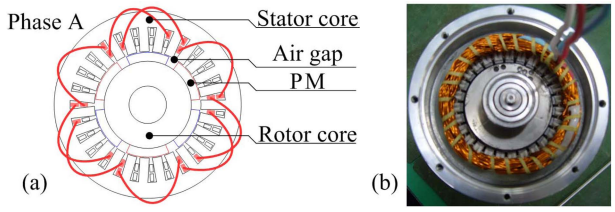

Fig. 1. (Color online) (a) Schematic and (b) photograph of the actual fixture model of an SPM motor having a 6-pole rotor and 27-slot stator.

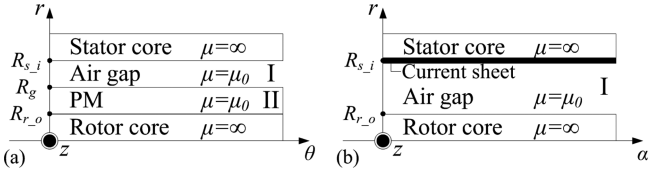

Fig. 2. Analytical model for the prediction of magnetic fields produced by (a) PMs and (b) stator windings.

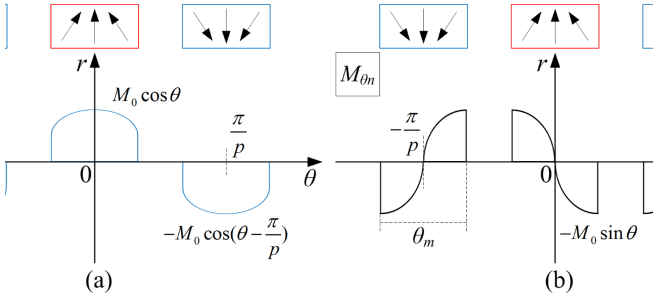

Fig. 3. (Color online) Parallel magnetization model for Fourier series expansion of the PMs.

and $M_0 = B_r/\mu_0$, B_r is the residual flux density of the PMs. $\mathbf{M}$ is the magnetization of the parallel magnetized PMs and can be obtained as follows:

$$\mathbf{M} = \sum_{n=-\infty}^{\infty} \left\{ M_{rn} e^{-jnp\theta} \mathbf{i}_r + M_{\theta n} e^{-jnp\theta} \mathbf{i}_\theta \right\} \tag{2}$$

Here, p and n denote the number of pole-pairs and the n^{th}-order space harmonic, respectively. Further, the PMs having parallel magnetization have radial and circumferential directions. M_{rn} and $M_{\theta n}$ are the n^{th}-order Fourier coefficients for radial and tangential magnetization distribution and can be expressed as

$$\begin{aligned} M_{rn} &= \frac{M_0}{\frac{\pi}{p}\{1-(np)^2\}} \left\{ e^{jnp\frac{\theta_m}{2}} \left(\sin\frac{\theta_m}{2} + jnp\cos\frac{\theta_m}{2} \right) \right. \\ &\qquad \left. - e^{-jnp\frac{\theta_m}{2}} \left(-\sin\frac{\theta_m}{2} + jnp\cos\frac{\theta_m}{2} \right) \right\} \\ M_{\theta n} &= \frac{M_0}{\frac{\pi}{p}\{1-(np)^2\}} \left\{ e^{jnp\frac{\theta_m}{2}} \left(\cos\frac{\theta_m}{2} - jnp\sin\frac{\theta_m}{2} \right) \right. \\ &\qquad \left. - e^{-jnp\frac{\theta_m}{2}} \left(\cos\frac{\theta_m}{2} + jnp\sin\frac{\theta_m}{2} \right) \right\} \end{aligned} \tag{3}$$

and because the vector potential has a z-axial component, $\mathbf{A}^{pm} = A^{pm}(r) e^{-jnp\theta} \mathbf{i}_z$. Thus, the solutions for the Laplace's and Poisson's equations from (1) can be obtained as follows:

$$\begin{aligned} \mathbf{A}^{pm\mathrm{I}} &= \sum_{n=-\infty,odd}^{\infty} \left(A_n^{\ I} r^{np} + B_n^{\ I} r^{-np} \right) e^{-jnp\theta} \mathbf{i}_z \\ \mathbf{A}^{pm\mathrm{II}} &= \sum_{n=-\infty,odd}^{\infty} \left\{ A_n^{\ II} r^{np} + B_n^{\ II} r^{-np} \right. \\ &\qquad \left. + \frac{\mu_0 npr}{(np)^2 - 1} \left(\frac{M_{\theta n}}{np} + jM_{rn} \right) \right\} e^{-jnp\theta} \mathbf{i}_z \end{aligned} \tag{4}$$

In conclusion, by substituting (4) in the definition of the magnetic vector potential, the radial and tangential flux densities generated by the PMs can be obtained as

$$\mathbf{B}_{\mathbf{rn}}^{pm\mathbf{I}} = -\sum_{n=-\infty,odd}^{\infty} \frac{jnp}{r}\left(A_n^{\ I} r^{np} + B_n^{\ I} r^{-np}\right) e^{-jnp\theta}\mathbf{i}_{\mathbf{r}}$$

$$\mathbf{B}_{\mathbf{rn}}^{pm\mathbf{II}} = -\sum_{n=-\infty,odd}^{\infty} \frac{jnp}{r}\left\{A_n^{\ II} r^{np} + B_n^{\ II} r^{-np} + \frac{\mu_0 npr}{(np)^2-1}\left(\frac{M_{\theta n}}{np} + jM_{rn}\right)\right\} e^{-jnp\theta}\mathbf{i}_{\mathbf{r}}$$

$$\mathbf{B}_{\boldsymbol{\theta}\mathbf{n}}^{pm\mathbf{I}} = -\sum_{n=-\infty,odd}^{\infty} np\left(A_n^{\ I} r^{np-1} - B_n^{\ I} r^{-np-1}\right) e^{-jnp\theta}\mathbf{i}_{\boldsymbol{\theta}} \tag{5}$$

$$\mathbf{B}_{\boldsymbol{\theta}\mathbf{n}}^{pm\mathbf{II}} = -\sum_{n=-\infty,odd}^{\infty} np\left\{A_n^{\ II} r^{np-1} - B_n^{\ II} r^{-np-1} + \frac{\mu_0}{(np)^2-1}\left(\frac{M_{\theta n}}{np} + jM_{rn}\right)\right\} e^{-jnp\theta}\mathbf{i}_{\boldsymbol{\theta}}$$

Here, the undetermined coefficients $A_n^{\ I}$, $B_n^{\ I}$, $A_n^{\ II}$, and $B_n^{\ II}$ can be easily resolved by applying suitable boundary conditions to (5).

2.3. Magnetic Fields Produced by Stator Windings

Figure 4 shows the current density distribution model of Fourier series expansion of the three-phase stator windings. Here, t_0 and τ_t denote the stator tooth width angle and the slot pitch, respectively. Further, S_0/R_{s_i} is the angle of the slot opening, where S_0 is the slot opening width. The current density distribution in phase A is expressed from Fig. 4 as

$$\mathbf{J}_{\mathbf{a}} = \sum_{n=-\infty,odd}^{\infty} I_n i_a e^{-jnp\alpha} \tag{6}$$

Here, I_n is the n^{th}-order Fourier coefficient of the current density distribution in phase A. The three-phase stator windings have a phase difference of $2\pi/3$ as electrical angle. Therefore, the current density distributions of B and C phases are obtained as follows:

$$\mathbf{J}_{\mathbf{b}} = \sum_{n=-\infty,odd}^{\infty} I_n i_b e^{-jnp\left(\alpha+\frac{2\pi}{3}\right)}$$

$$\mathbf{J}_{\mathbf{c}} = \sum_{n=-\infty,odd}^{\infty} I_n i_c e^{-jnp\left(\alpha-\frac{2\pi}{3}\right)} \tag{7}$$

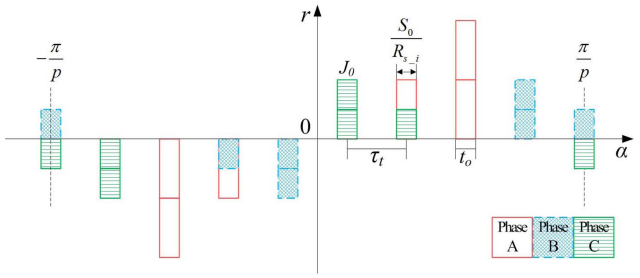

Fig. 4. (Color online) Current density model for Fourier series expansion of the stator coils.

where i_a, i_b, and i_c are the current amplitudes of each phase. Similar to the magnetic field analysis of the PMs using the magnetic vector potential, the Coulomb gauge, and Laplace's equations, the governing equation for the armature reaction field generated by the stator windings from Fig. 2(b) is $\nabla^2\mathbf{A}^{sw\mathbf{I}} = 0$. We assumed that the current of the stator windings is distributed as a current sheet. Therefore, the three-phase current is considered at the boundary condition. From the definition of the magnetic vector potential, the flux density of phase A for the armature reaction field can be obtained as

$$\mathbf{B}_{\mathbf{rn}}^{\ sw\_a} = -\sum_{n=-\infty,odd}^{\infty} \frac{jnp}{r}\left(C_n r^{np} + D_n r^{-np}\right) e^{-jnp\alpha}\mathbf{i}_{\mathbf{r}}$$

$$\mathbf{B}_{\boldsymbol{\alpha}\mathbf{n}}^{\ sw\_a} = -\sum_{n=-\infty,odd}^{\infty} np\left(C_n r^{np-1} - D_n r^{-np-1}\right) e^{-jnp\alpha}\mathbf{i}_{\boldsymbol{\alpha}} \tag{8}$$

Here, the undetermined coefficients C_n, and D_n can be determined by applying suitable boundary conditions to (8). Thus, the flux density produced by the three-phase stator windings can be given as follows:

$$\begin{aligned}\mathbf{B}_{\mathbf{rn}}^{\ sw} &= \mathbf{B}_{\mathbf{rn}}^{\ sw\_a} + \mathbf{B}_{\mathbf{rn}}^{\ sw\_b} + \mathbf{B}_{\mathbf{rn}}^{\ sw\_c} \\ &= -\sum_{n=-\infty,odd}^{\infty} \frac{jnp}{r} D_{n\_I}\left(R_{r\_o}^{\ -2np} r^{np} + r^{-np}\right) \\ &\quad \cdot\left(i_a e^{-jnp\alpha} + i_b e^{-jnp\left(\alpha+\frac{2\pi}{3}\right)} + i_c e^{-jnp\left(\alpha-\frac{2\pi}{3}\right)}\right)\mathbf{i}_{\mathbf{r}} \\ \mathbf{B}_{\boldsymbol{\alpha}\mathbf{n}}^{\ sw} &= \mathbf{B}_{\boldsymbol{\alpha}\mathbf{n}}^{\ sw\_a} + \mathbf{B}_{\boldsymbol{\alpha}\mathbf{n}}^{\ sw\_b} + \mathbf{B}_{\boldsymbol{\alpha}\mathbf{n}}^{\ sw\_c} \\ &= -\sum_{n=-\infty,odd}^{\infty} npD_{n\_I}\left(R_{r\_o}^{\ -2np} r^{np-1} - r^{-np-1}\right) \\ &\quad \cdot\left(i_a e^{-jnp\alpha} + i_b e^{-jnp\left(\alpha+\frac{2\pi}{3}\right)} + i_c e^{-jnp\left(\alpha-\frac{2\pi}{3}\right)}\right)\mathbf{i}_{\boldsymbol{\alpha}}\end{aligned} \tag{9}$$

2.4. Back-emf and Electromagnetic Torque Calculations

The stator coil flux linkage per turn of one phase produced by the PMs is given by $\Phi = B{\cdot}S$. Here, B and S denote the flux density in the air gap caused by the PMs and area of flux linkage passed, respectively. From (5), the flux density can be rewritten as

$$\begin{aligned}B_{pm} &= -\sum_{n=-\infty,odd}^{\infty} jnp\left(A_n^{\ I} r^{np-1} + B_n^{\ I} r^{-np-1}\right) e^{-jnp\theta} \\ &= \sum_{n=-\infty,odd}^{\infty} B_e e^{-jnp\theta} = \sum_{n=-\infty,odd}^{\infty} B_e e^{-jnp(\alpha+\omega_r t)}\end{aligned} \tag{10}$$

Thus, the flux linkage of one turn is given as follows

$$\Phi_{pm} = \int_{-\frac{\alpha_y}{2}}^{\frac{\alpha_y}{2}} B_{pm}(r,\alpha) R_s l_a d\alpha \tag{11}$$

Here, α_y and l_a denote the winding pitch angle and axial length of the SPM motor, respectively. Hence, the induced back-emf voltage per coil of one phase is expressed from (11) as

$$e = -N\frac{d\Phi_{pm}}{dt} = 2NB_e R_s l_a K_{pn}\omega_r \sin(np\omega_r t) \tag{12}$$

where N is the number of turns per coil, and K_{pn} is the winding pitch factor, $K_p = \sin(np\cdot\alpha_y/2)$. From the back-emf voltage induced in one phase, the back-emf induced in the three phases can be obtained as

$$\begin{aligned} e_a &= 2NB_e R_s l_a K_{dpn}\omega_r \sin(np\omega_r t) \\ e_b &= 2NB_e R_s l_a K_{dpn}\omega_r \sin\left\{n\left(p\omega_r t + \frac{2\pi}{3}\right)\right\} \\ e_c &= 2NB_e R_s l_a K_{dpn}\omega_r \sin\left\{n\left(p\omega_r t - \frac{2\pi}{3}\right)\right\} \end{aligned} \tag{13}$$

Here, $K_{dpn} = K_{dn}K_{pn}$ is the winding factor, and K_{dn} is the winding distribution factor [7].

The electromagnetic torque can be calculated from the three-phase winding back-emf and input current. For the three phases, currents with amplitude I_1 are given as

$$\begin{aligned} i_a &= I_1 \sin\left(p\omega_r t\right) \\ i_b &= I_1 \sin\left(p\omega_r t + \frac{2\pi}{3}\right) \\ i_c &= I_1 \sin\left(p\omega_r t - \frac{2\pi}{3}\right) \end{aligned} \tag{14}$$

However, for the SPM motor, various losses should be considered. Figure 5 shows the equivalent circuit of one phase of the SPM motor. Here, R_a and X_a are the resistance and reactance of the SPM motor, and V_a is the effective terminal voltage. Further, e_{back} and I_a denote the back-emf and phase current that can be obtained from (13) and (14), respectively. P_m is the output power of the SPM motor, and P_{FW} denotes mechanical losses such as bearing friction (P_{fr}) and windage loss (P_{wind}) and is given by $P_{FW} = P_{fr} + P_{wind}$. These losses can be evaluated as [8]

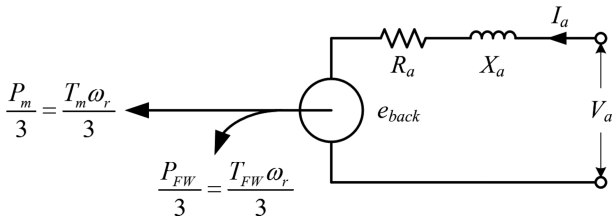

Fig. 5. Equivalent circuit of one phase of the SPM motor.

$$\begin{aligned} P_{fr} &= k_{fr} G_r n_r \times 10^{-3} \quad [\mathrm{W}] \\ P_{wind} &= 2D_{rout}{}^3 l_a n_r{}^3 \times 10^{-6} \quad [\mathrm{W}] \end{aligned} \tag{15}$$

where k_{fr} = 1-3, and G_r and n_r are the mass of the rotor in kg and rotational speed in rpm. Further, D_{rout} is the outer diameter of the rotor. The torques corresponding to the output power and mechanical losses are denoted by T_m and T_{FW}, respectively. Neglecting mechanical losses, the output power (P_o) of the SPM motor can be given as

$$P_o = T_o\omega_r = e_a i_a + e_b i_b + e_c i_c \tag{16}$$

Thus, the electromagnetic torque, considering the mechanical losses, of the SPM motor is expressed as

$$T_m = T_o - T_{FW} = \frac{1}{\omega_r}\left\{P_o - P_{FW}\right\} \tag{17}$$

3. Results and Discussion

3.1. Magnetic Field Distribution due to PMs and Stator Winding Currents

Figure 6 shows the magnetic flux line distribution pro-

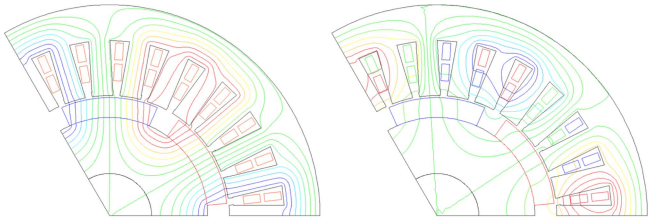

Fig. 6. (Color online) Magnetic flux line distribution produced by (a) PMs and (b) stator winding currents.

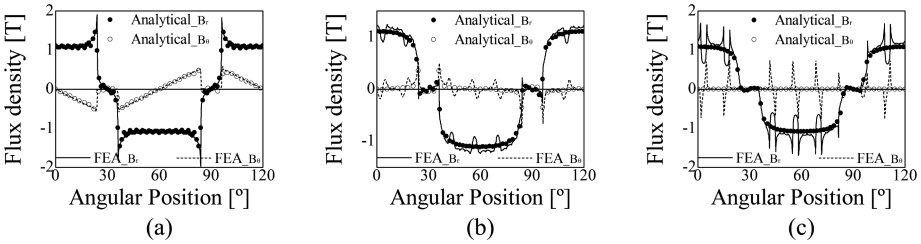

Fig. 7. Comparison of analytical results without slotting effects with FE results with slotting effects for flux density produced by PMs at various radius: (a) R_{r_o} (b) R_g (c) R_{s_i}.

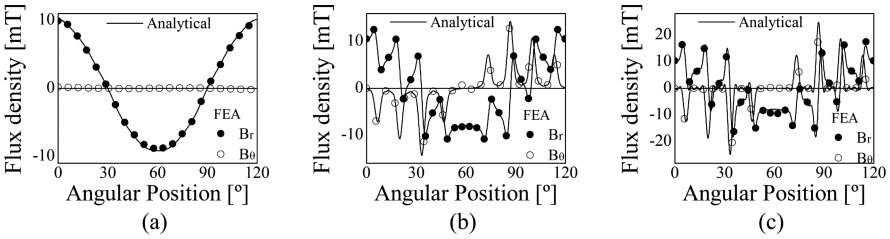

Fig. 8. Comparison of analytical results with FE results for flux density produced by stator winding currents for (a) R_{r_o}, (b) R_g, and (c) R_{s_i}.

duced by the PMs and stator winding currents obtained from the 2-D nonlinear FE analysis. As shown in Fig. 6, the PMs of our model are parallel magnetized and the stator windings are not symmetrical about a phase.

Figure 7 shows a comparison of the analytical results without slotting effects with FE result with slotting effects for flux density produced by the PMs about the mechanical angular position at different radii R_{r_o}, R_g, and R_{s_i}. It is noted that effective air-gap length for analytical model is corrected by introducing Carter's coefficient given by $g_e = g + (K_c - 1)(g + H_m/\mu_r)$. Here g, H_m, and μ_r are the air-gap length, the magnet thickness and the relative permeability of the PMs, respectively, and K_c is the Carter's coefficient whose formula is given in ref. 9. Due to slotting effects, it can be seen that the analytical results are not shown in good agreement with FE results. However, it can be predicted that total flux linking with the stator coils calculated by analytical method makes little difference from that calculated by FE method. Therefore, analytical results will be shown in good agreement with FE results for back-emf and torque.

Further, a comparison of the analytical and nonlinear FE results of the flux density produced by the stator winding currents at different radii is shown in Fig. 8. The flux density generated by the stator windings is much lesser than that generated by the PMs. The analytical results are shown to be in good agreement with the 2-D nonlinear FE results.

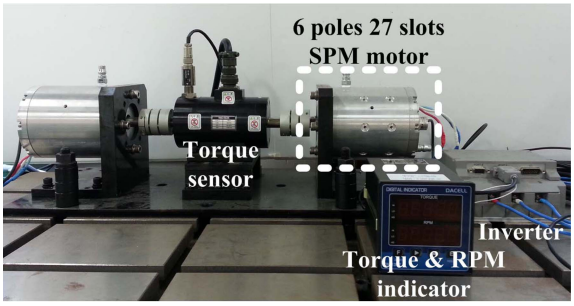

Fig. 9. (Color online) Testing apparatus for back-emf and electromagnetic torque measurements of the SPM motor.

3.2. Back-emf and Electromagnetic Torque

Figure 9 illustrates the apparatus used for testing the back-emf and electromagnetic torque of the SPM motor. For measuring the back-emf, the shaft of the SPM motor is connected to the shaft of another generator.

Figures 10(a) and 10(b) show the comparison of the analytical results with the nonlinear FE calculations and measurements for the back-emf of the SPM motor, respectively. The analytical results are shown to be in good agreement with the nonlinear FE results and measurements. Moreover, the amplitude of the current and rotor speed are set to be 22 A and 6540 rpm, respectively.

A comparison of the analytical results with the nonlinear FE and experimental results for electromagnetic torque is shown in Fig. 11. The electromagnetic torque is measured at a rotational speed of 6540 rpm. The analy-

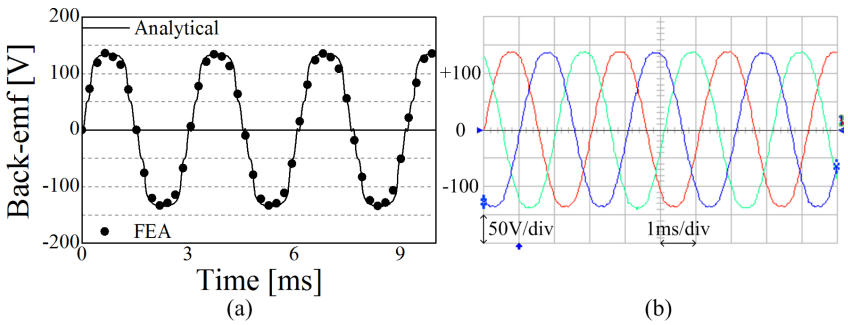

Fig. 10. (Color online) Back-EMF at 6540 rpm: (a) comparison of analytical results with FE results and (b) measurements.

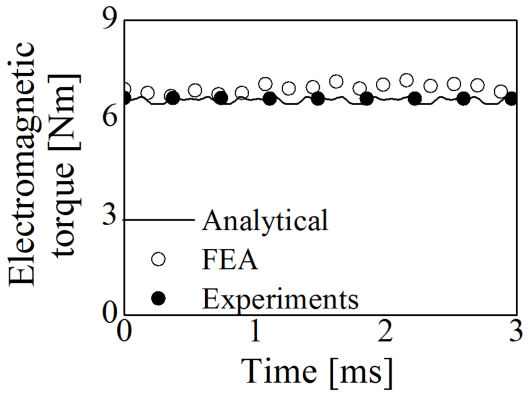

Fig. 11. Comparison of analytical results with FE calculations and measurements for electromagnetic torque at 6540 rpm.

tical results calculated from (17) are in good agreement with measurements at k_{fr} = 2. However, the nonlinear FE results without considering friction and windage losses of (15) are slightly different from the analytical and experimental results.

4. Conclusion

This paper presents the electromagnetic properties of a parallel magnetized SPM motor having asymmetric windings, based on analytical magnetic field calculations. The analytical solutions of the magnetic fields produced by the PMs and stator windings are computed using the space harmonic method. The analytical prediction results correspond well with the 2-D nonlinear FE analysis results. Thus, the validity of this analysis is confirmed. Further, electromagnetic analysis including flux linkage due to PMs, back-emf, and electromagnetic torque is obtained from these analytical solutions. The experimental results of the actual fixture model having 6-poles and 27-slots are also shown to be in good agreement with the analytical and nonlinear FE results. In this paper, the slotting effect is not taken into account. However, the electromagnetic performance of an SPM motor with a slotted stator can be calculated by applying the same process considering the permeance function for the slotting effect. Finally, the efficiency of the SPM motor with a fractional slot/pole number combination can be improved by calculating the inductance, normal force, and cogging torque based on mentioned analysis in this paper.

Acknowledgements

This research was supported by the basic science research program through the National Research Foundation of Korea (NRF) funded by the Ministry of Education, Science, and Technology under Grant 2011-0013398 and in part by a grant from Human Resources Development of the Korea Institute of Energy Technology Evaluation and Planning (KETEP) funded by the Korean government's Ministry of Knowledge Economy under Grant 20124030200090.

References

[1] Z. Q. Zhu and D. Howe, Proc. IEEE **95**, 746 (2007).
[2] S. C. Yang, T. Suzuki, R. D. Lorenz, and T. M Jahns, IEEE Trans. Ind. Appl. **47**, 2103 (2011).
[3] A. M. EL-Refaie, IEEE Trans. Ind. Electron. **57**, 107 (2010).
[4] Z. Q. Zhu, Ecologic Vehicles Renewable Energies (2009).
[5] N. Bianchi, IEEE Industry Applications Conf. **1**, 21 (2000).
[6] Z. Q. Zhu, D. Howe, and C. C. Chan, IEEE Trans. Magn. **38**, 229 (2002).
[7] Z. Q. Zhu and D. Howe, IEEE Trans. Magn. **29**, 152 (1993).
[8] Jacek F. Gieras and Mitchell Wing, Marcel Dekker Inc. New York (2002) pp. 571-572.
[9] Z. Q. Zhu and D. Howe, IEEE Trans. Magn. **29**, 1, 143 (1993).